

AD-A261 903



USAFA-TR-92-4

2

ANOTHER LOOK AT THE
DRIVEN CAVITY PROBLEM



MAX A. STAFFORD, LT COL, USAF

DEPT OF MATHEMATICAL SCIENCES

NOVEMBER 1992

FINAL REPORT

APPROVED FOR PUBLIC RELEASE; DISTRIBUTION UNLIMITED



DEAN OF THE FACULTY
UNITED STATES AIR FORCE ACADEMY
COLORADO 80840

93-05151



4178

98 3 10 082

ANOTHER LOOK AT THE DRIVEN CAVITY PROBLEM

BY

Lt Col Max A. Stafford

Department of Mathematical Sciences

DTIC C-111111 UNCLASSIFIED 1

Accession For	
NTIS CRA&I	<input checked="checked" type="checkbox"/>
DTIC TAB	<input type="checkbox"/>
Unannounced	<input type="checkbox"/>
Justification	
By	
Distribution /	
Availability Codes	
Dist	Avail and/or Special
A-1	

TABLE OF CONTENTS

<u>SECTION</u>	<u>TITLE</u>	<u>PAGE</u>
1	Introduction and Problem Description.....	1
2	Applying the Method of Lines to Partial Differential Equations.....	4
3	Solutions to the Driven Cavity Problem by Conventional Methods.....	10
4	Solution by Use of the Matrix Exponential.....	13
5	Spectrum Analysis of the Coefficient Matrix.....	15
6	Conclusion.....	24
	References.....	27
Appendix A	Equations Arising from the Method of Lines Applied to the Driven Cavity Problem.....	28
Appendix B	Approximate Solutions to the Driven Cavity Problem.....	33

Technical Review by Lt Col Wayne Hallgren
Department of Aeronautics
USAF Academy, Colorado 80840

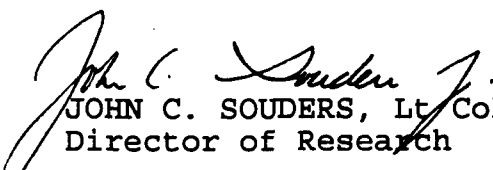
Technical Review by Captain Bruce DeBlois
Department of Mathematical Sciences
USAF Academy, Colorado 80840

Editorial Review by Lt Col Bruce Degi
Department of English
USAF Academy, Colorado 80840

This research report entitled "Another Look at the Driven Cavity Problem" is presented as a competent treatment of the subject, worthy of publication. The United States Air Force Academy vouches for the quality of the research, without necessarily endorsing the opinions and conclusions of the author.

This report has been cleared for further dissemination only as directed by the Dean of the Faculty or higher DOD authority in accordance with AFR 80-45 and DOD 5200.1-R. Reproduction is authorized to accomplish an official government purpose.

This research report has been reviewed and approved for publication by the sponsor agency.


JOHN C. SOUDERS, Lt Col, USAF
Director of Research

2 November 1992
Dated

REPORT DOCUMENTATION PAGE			Form Approved OMB No 0704-0188	
<small>Public reporting burden for this collection of information is estimated to average 1 hour per response, including the time for reviewing instructions, searching existing data sources, gathering and maintaining the data needed, and completing and reviewing the collection of information. Send comments regarding this burden estimate or any other aspect of this collection of information, including suggestions for reducing this burden, to Washington Headquarters Services, Directorate for Information Operations and Reports, 1215 Jefferson Davis Highway, Suite 1204, Arlington, VA 22202-4302, and to the Office of Management and Budget, Paperwork Reduction Project (0704-0188), Washington, DC 20503.</small>				
1. AGENCY USE ONLY (Leave blank)		2. REPORT DATE 2 NOV 92	3. REPORT TYPE AND DATES COVERED Final	
4. TITLE AND SUBTITLE Another Look at the Driven Cavity Problem			5. FUNDING NUMBERS	
6. AUTHOR(S) Max A. Stafford, Lt Col, USAF				
7. PERFORMING ORGANIZATION NAME(S) AND ADDRESS(ES) Department of Mathematical Sciences United States Air Force Academy, Colorado 80840			8. PERFORMING ORGANIZATION REPORT NUMBER USAF-A-TR-92-4	
9. SPONSORING/MONITORING AGENCY NAME(S) AND ADDRESS(ES)			10. SPONSORING/MONITORING AGENCY REPORT NUMBER	
11. SUPPLEMENTARY NOTES				
12a. DISTRIBUTION/AVAILABILITY STATEMENT			12b. DISTRIBUTION CODE	
13. ABSTRACT (Maximum 200 words) Numerical analysis of a lid driven cavity is a standard computational fluid dynamics problem. A semi-discrete method known as the method of lines is used in this report to reduce the problem to one of solving a coupled system of first-order linear differential equations and linear algebraic equations. The spectrum of the coefficient matrix in the first-order system of differential equations is analyzed as the flow field evolves from rest to steady state. By examining the pattern of this eigenvalue migration it is possible to estimate the time to steady state by using very coarse grids. A simple relationship between the Reynolds number and time to steady state is also apparent from analyzing the coefficient matrix.				
14. SUBJECT TERMS Computational fluid dynamics, spectral analysis, driven cavity problem, method of lines			15. NUMBER OF PAGES 35	
			16. PRICE CODE	
17. SECURITY CLASSIFICATION OF REPORT UNCLASSIFIED	18. SECURITY CLASSIFICATION OF THIS PAGE UNCLASSIFIED	19. SECURITY CLASSIFICATION OF ABSTRACT UNCLASSIFIED	20. LIMITATION OF ABSTRACT	

Section 1

INTRODUCTION AND PROBLEM DESCRIPTION

Background

In 1991 Dr. John Shoosmith, a researcher at the National Aeronautics and Space Administration (NASA), proposed a new method for solving systems of first-order differential equations in parallel. He presented his method and a one-dimensional application of the algorithm to the 1991 International Conference on Industrial and Applied Mathematics held in Washington, DC. His original research proposal indicated plans to apply the method to a two-dimensional test case such as the driven cavity problem (DCP). The research documented in this report originated out of an attempt to apply his algorithm to the DCP. It is shown herein that Dr. Shoosmith's method cannot solve the DCP. In the course of the investigation additional results, some of which may be new, were obtained.

The driven cavity problem is a standard problem in computational fluid dynamics. A National Aeronautics and Space Administration publication in 1975 [Rubin] cites 10 articles on the subject during the period 1965 through 1974. This same publication documents DCP solutions obtained by eight research teams working in coordination with NASA. The computations were typically performed on a CDC 6400 mainframe computer for the purpose of comparing different approaches. Undoubtedly many other papers on the DCP have made their way into the literature since the writing of that publication. The primary advantage of using this problem is that it is simple to describe but the solution is fairly complicated and captures many salient features of fluid flow phenomena. Another advantage is that accurate solutions are readily available for comparison.

If successful, Dr. Shoosmith's proposed method for solving large systems of first-order differential equations would make use of parallel computation by distributing eigenvector evaluations associated with an n th-order matrix to n parallel processors. The strength of the method is its ability to perform the eigenvector computation efficiently, but the method requires the matrix to have real, distinct eigenvalues. His one-dimensional test case provided a solution to Burger's equation and the associated matrix did in fact have real, distinct eigenvalues. It is shown in this report, however, that the spectrum

of the matrix arising in the driven cavity problem contains complex eigenvalues and, unfortunately, Dr. Shoosmith's method cannot provide a solution. While investigating this problem, however, it was found that by computing the spectrum of the matrix associated with a very coarse grid one can gain considerable information about the solution. It is this observation which may be new and of interest to practicing computational fluid dynamicists.

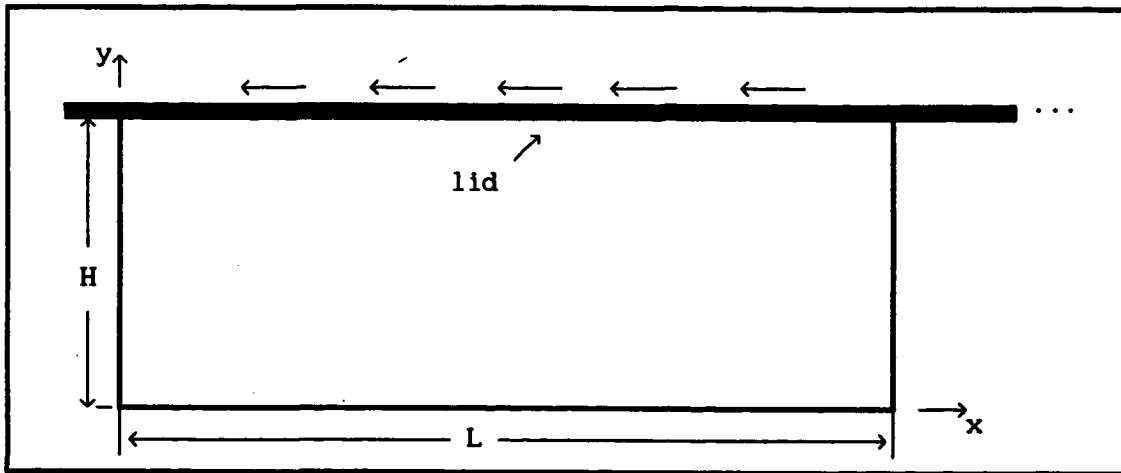


Figure 1: Geometry of the Driven Cavity

The Driven Cavity Problem

Consider a rectangular cavity (Figure 1) with fixed sides and bottom which contains a viscous, incompressible fluid. Along the top edge of the cavity a flat surface, the "lid," capable of translating to the left is in contact with the fluid. At time t_0 the lid instantaneously begins movement to the left at a constant speed, U . The Navier-Stokes equations in the stream function-vorticity formulation are [Ames]:

$$\zeta_t = -\psi_y \zeta_x + \psi_x \zeta_y + \frac{1}{R} (\zeta_{xx} + \zeta_{yy}) \quad (1)$$

$$\psi_{xx} + \psi_{yy} = -\zeta \quad (2)$$

where ζ (vorticity) and ψ (stream function) are related to the x and y

velocity components (u,v) at every point within the cavity by

$$u = \psi_y \qquad v = -\psi_x \qquad \zeta = v_x - u_y$$

For purposes of this report, the driven cavity problem is defined as follows:

If at time $t = 0$ the velocity everywhere within the cavity is zero, determine ζ and ψ at every point within the cavity for all time greater than $t = 0$.

Additionally, in this report the length and width of the cavity are one distance unit and the lid speed is one distance unit per unit time. With these values the Reynolds number, $R = UL/\nu$, becomes simply $1/\nu$ where ν is the fluid's kinematic viscosity.

Overview of Report

The following section describes how the partial differential equation for vorticity, ζ , is converted into a system of ordinary differential equations. Section 3 provides solutions to the driven cavity problem obtained by use of conventional methods. Dr. Shoosmith's method for solving the coupled system of ordinary differential equations is outlined in Section 4. In Section 5 the spectral properties of the coefficient matrix are presented and discussed. The initial eigenvalues and their migration during the time evolution of the solution are remarkable because they strongly indicate that complex eigenvalues arise in all numerical solutions of the DCP and thus the method of Dr. Shoosmith cannot be applied. Further interesting consequences of the eigenvalues of A and their migration as the solution proceeds to steady state are discussed as well. Section 6 contains some concluding remarks including suggestions on further research.

Computational Equipment and Software

All computations were performed on a personal computer, a Unisys Series 800/20C with an 80386 CPU and an 80387 coprocessor. The programs were written using Borland's Turbo Pascal Version 6, and are available from the author upon request.

Section 2

Applying the Method of Lines to the Partial Differential Equation

The method of lines is a semi-discrete method which is sometimes used to solve partial differential equations [Ames]. The basic idea is to discretize all independent variables but one, thus converting the system of partial differential equations into a system of ordinary differential equations. The driven cavity problem is amenable to this approach.

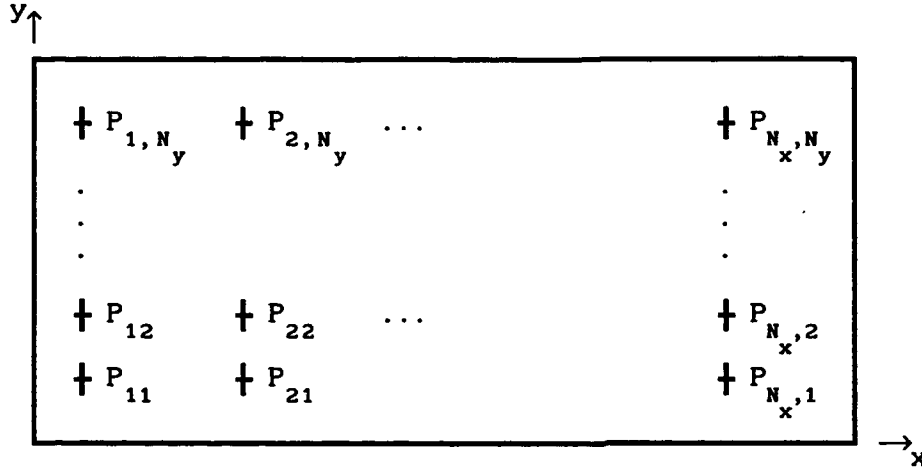


Figure 2: Grid for Driven Cavity Problem

The method of lines requires a discretization of two of the three independent variables and the usual procedure is to select these to be the spatial variables. Consider a regular grid superimposed on the interior of the cavity as depicted in Figure 2. We denote the number of interior points on any given row by N_x , and the number of interior points on any given column by N_y . The points are labeled such that the point $P_{i,j}$ is located at $x = i\Delta x$, $y = j\Delta y$. Discretization gives rise to new dependent variables at each grid point:

$$\zeta_\ell = \zeta(i\Delta x, j\Delta y) \quad \psi_\ell = \psi(i\Delta x, j\Delta y)$$

where

$$\ell = (i - 1)N_x + j$$

Note that this numbering system produces $n = N_x N_y$ new variables to represent both ζ and ψ . It is convenient to slightly abuse the notation and define the column vectors of these new unknowns as follows:

$$\zeta = \begin{bmatrix} \zeta_1 \\ \vdots \\ \zeta_n \end{bmatrix} \quad \psi = \begin{bmatrix} \psi_1 \\ \vdots \\ \psi_n \end{bmatrix}$$

It is straightforward, now, to approximate both first and second-order derivatives appearing in the first of the stream function-vorticity equations (Equation 1) and thereby create a system of first-order ordinary differential equations in ζ :

$$\dot{\zeta} = A(\psi)\zeta + \gamma(\psi) \quad (3)$$

where $A(\psi)$ is an n^{th} -order matrix and $\gamma(\psi)$ is a column vector with n rows.

The derivation of each of these will be discussed below.

Again using finite differences to approximate second-order derivatives, we have in lieu of Poisson's equation (Equation 2) a linear algebraic system of equations:

$$D\psi = -\zeta \quad (4)$$

where D is a constant n^{th} -order matrix whose specific values will be derived below. It is clear, now, that we must solve a coupled system of equations, one a system of first-order ordinary differential equations and the other a linear algebraic system of equations.

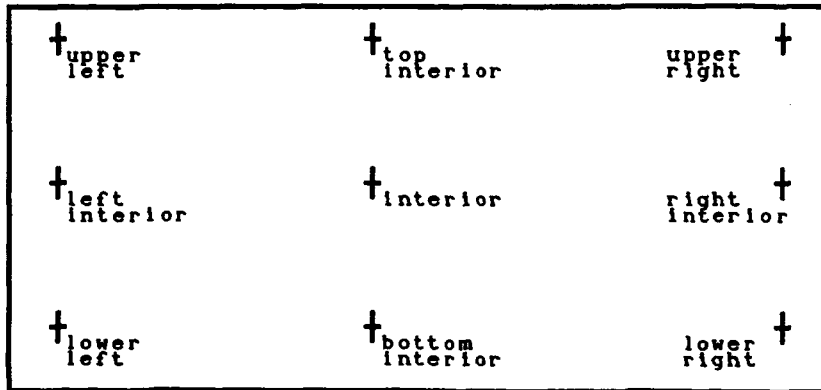


Figure 3: Node Types for Driven Cavity Grid

Determination of the components of the $A(\psi)$ matrix is straightforward but a bit tedious due to the many different cases to consider. There are, in fact, nine separate situations which can occur as Figure 3 depicts. A sample derivation for one of these cases, the top center, is now presented and the results of similar derivations for the other eight possibilities are presented in Appendix A.

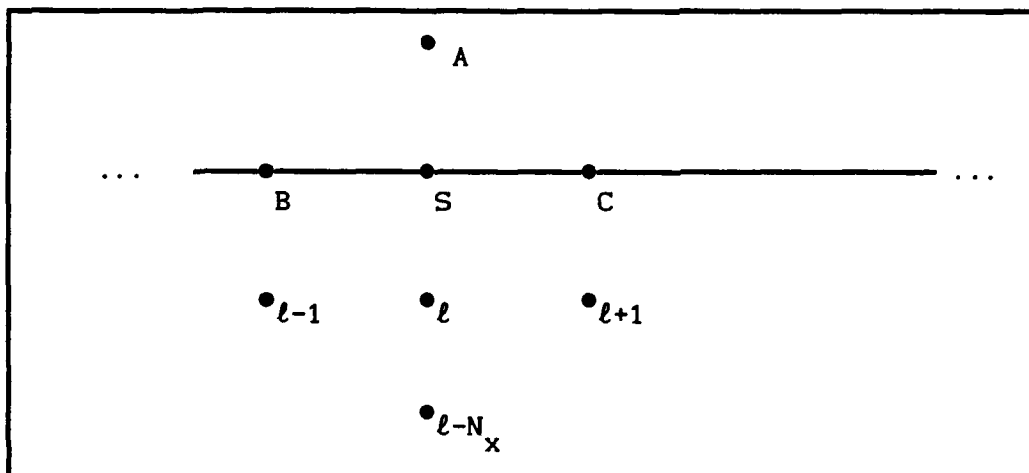


Figure 4: Top Interior Grid Point

Consider the grid points around a general node on the top row, as depicted in Figure 4. Using central differences for the spatial partial derivatives yields the following $O(h^2)$ semi-discrete equation at node ℓ :

$$\begin{aligned} \dot{\zeta}_\ell = & - \left[\frac{\psi_S - \psi_{\ell-N_x}}{2\Delta y} \right] \left[\frac{\zeta_{\ell+1} - \zeta_{\ell-1}}{2\Delta x} \right] + \left[\frac{\psi_{\ell+1} - \psi_{\ell-1}}{2\Delta x} \right] \left[\frac{\zeta_S - \zeta_{\ell-N_x}}{2\Delta y} \right] \\ & + \frac{1}{R} \left[\frac{\zeta_{\ell-1} - 2\zeta_\ell + \zeta_{\ell+1}}{\Delta x^2} + \frac{\zeta_{\ell-N_x} - 2\zeta_\ell + \zeta_S}{\Delta y^2} \right] \end{aligned}$$

We need to invoke the boundary conditions, now, to determine ψ_S and ζ_S . We let $\psi = 0$ on the entire boundary, but ζ_S must be determined. We assume a no slip condition at the fluid-lid interface, so

$$u_S = \left. \frac{\partial \psi}{\partial y} \right|_S = -1$$

A fictitious node at A is now introduced so that

$$\left. \frac{\partial \psi}{\partial y} \right|_S \approx \frac{\psi_A - \psi_\ell}{2\Delta y} = -1$$

Thus,

$$\psi_A = \psi_\ell - 2\Delta y$$

An $O(h^2)$ discrete approximation to Poisson's equation at S is

$$\frac{\psi_B - 2\psi_S + \psi_C}{\Delta x^2} + \frac{\psi_\ell - 2\psi_S + \psi_A}{\Delta y^2} = -\zeta_S$$

This yields

$$\zeta_S = -2 \frac{\psi_\ell - \Delta y}{\Delta y^2}$$

Applying this result to the $\dot{\zeta}$ equation and performing some algebraic manipulation we obtain

$$\begin{aligned} \dot{\zeta}_\ell = & \left[\frac{-(\psi_{\ell+1} - \psi_{\ell-1})}{4\Delta x \Delta y} + \frac{1}{R\Delta y^2} \right] \zeta_{\ell-N_x} + \left[\frac{-\psi_{\ell-N_x}}{4\Delta x \Delta y} + \frac{1}{R\Delta x^2} \right] \zeta_{\ell-1} \\ & -2 \left[\frac{1}{R\Delta x^2} + \frac{1}{R\Delta y^2} \right] \zeta_\ell + \left[\frac{\psi_{\ell-N_x}}{4\Delta x \Delta y} + \frac{1}{R\Delta x^2} \right] \zeta_{\ell+1} \\ & - \left[\frac{(\psi_{\ell+1} - \psi_{\ell-1})(\psi_\ell - \Delta y)}{2\Delta x \Delta y^3} + \frac{\psi_\ell - \Delta y}{R\Delta y^4} \right] \end{aligned}$$

The terms multiplying $\zeta_{\ell-N_x}$, $\zeta_{\ell-1}$, ζ_ℓ , and $\zeta_{\ell+1}$ would be elements of $A(\psi)$ on row ℓ in columns $\ell-N_x$, $\ell-1$, ℓ , and $\ell+1$, respectively. The last term corresponds to the element in row ℓ of the $\gamma(\psi)$ vector.

The matrix D in the discretized Poisson equation is easier to derive because all terms are constant. The same nine cases occur, however, and each must be considered separately. For example, consider a general node in the extreme right column as depicted in Figure 5.

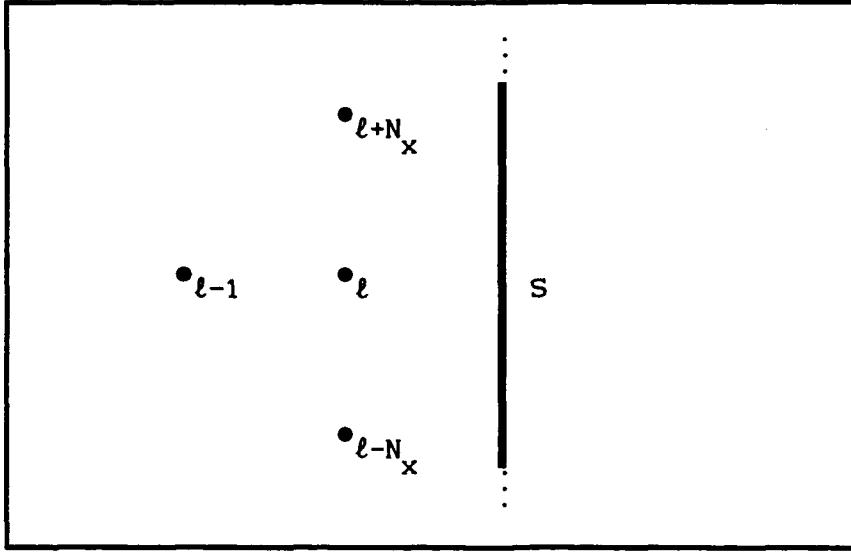


Figure 5: Right Interior Grid Point

The discretized Poisson equation, then, becomes

$$\frac{\psi_{\ell-1} - 2\psi_{\ell} + \psi_S}{\Delta x^2} + \frac{\psi_{\ell-N_x} - 2\psi_{\ell} + \psi_{\ell+N_x}}{\Delta y^2} = -\zeta_{\ell}$$

After some manipulation we have

$$\frac{1}{\Delta y^2} \psi_{\ell-N_x} + \frac{1}{\Delta x^2} \psi_{\ell-1} + \left(\frac{-2}{\Delta x^2} + \frac{-2}{\Delta y^2} \right) \psi_{\ell} + \frac{1}{\Delta y^2} \psi_{\ell+N_x} = -\zeta_{\ell}$$

The equations for all nine node types are summarized in Appendix A.

This concludes the translation of the partial differential equation into a system of ordinary differential equations and of Poisson's equation into an accompanying, coupled system of linear algebraic equations. In the following section, this system is solved by conventional means on grids with varying degrees of refinement.

Section 3

SOLUTIONS TO THE DRIVEN CAVITY PROBLEM BY CONVENTIONAL METHODS

The Method

In this section results from solving the two systems of equations derived above are presented. Those equations, repeated here for convenience, were

$$\dot{\zeta} = A(\psi)\zeta + \gamma(\psi) \quad (3)$$

$$D\psi = -\zeta \quad (4)$$

where $A(\psi)$ is a matrix of order n ($n = N_x N_y$) which depends upon the value of ψ , $\gamma(\psi)$ is a column vector with n components which also depends upon the value of ψ , and D is a constant matrix of order n . Detailed expressions for $A(\psi)$ and $\gamma(\psi)$ can be found in Appendix A.

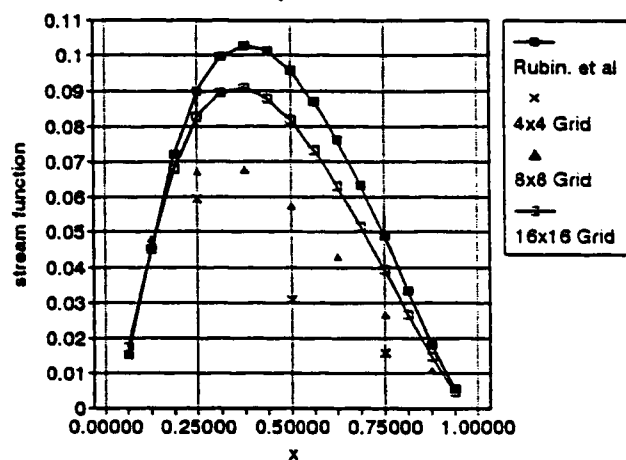
Solutions of Equations 3 and 4 were obtained by use of the classical fourth-order Runge-Kutta algorithm and the Gauss-Seidel iterative method, respectively. Initial values of zero were used for ζ and ψ . A single step of the procedure consisted simply of propagating forward one time step for ζ by Runge-Kutta, then solving for ψ by Gauss-Seidel to obtain the new value of ψ . This updated value was then used to modify $A(\psi)$ and $\gamma(\psi)$ and the next time step could then be taken. A fixed time step was used for each run of the program. A stopping time was established by allowing the process to run until a reasonably small value of the max norm of the right hand side of the vorticity equation was noted (typically 1×10^{-5}). It should be noted that far more efficient differential equation solvers and linear algebraic system solvers are available. The intent was not to solve the DCP in the most efficient manner, but merely to generate solutions which could be used to compute the spectrum of the coefficient matrix $A(\psi)$, and which could be compared with solutions generated by the method of Dr. Shoosmith.

Results

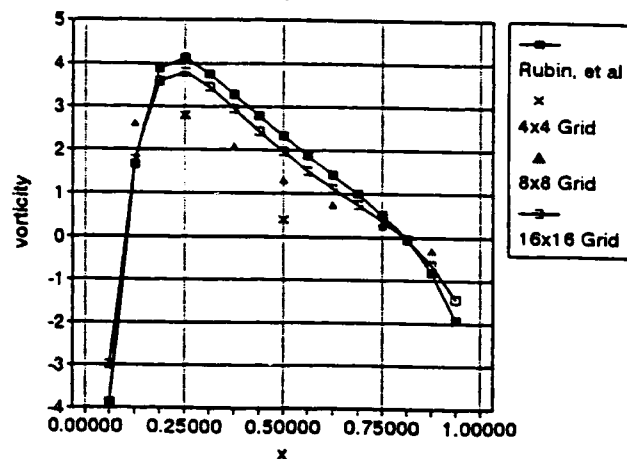
Validation of the solution method was accomplished by comparing ζ and ψ with published results. Memory limitations of Borland's Turbo Pascal and computer time limitations prevented runs with grids as fine as desired. However, by creating a series of three runs with successively finer grids it was possible to numerically validate the method. In Figure 6, graphs at three y locations ($y = 0.25$, $y = 0.5$, and $y = 0.75$) are presented for both ζ and ψ . Appendix B contains tabular listings of the results from this research. The number of intervals for the grids used in the present research are 4, 8, and 16 which correspond to $n = 9$, 49, and 225. In [Rubin] a grid with 64 intervals is used to determine ζ and ψ , and values for x and y increments of $1/16$ of a unit are published. These values are presented on the same graphs. It appears that as grids are made finer the values of ζ and ψ , computed by the method described above, approach the published values of Rubin. Finer grids could of course be used in order to be more certain that the solution technique in this research is accurate. The trend is sufficiently convincing, however, that spectral results given later in this report are believed to be reasonable.

A conventional technique for solving the DCP having been presented, along with results obtained from applying the technique, we turn now to the method of Dr. Shoosmith for solving systems of first-order ordinary differential equations.

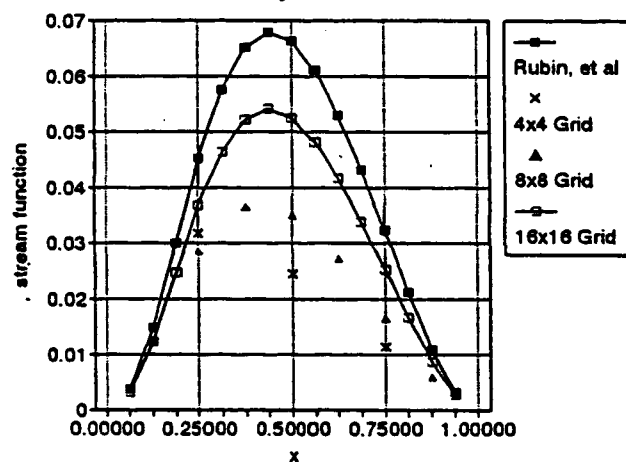
Stream Function versus x Position
at $y = 0.75$



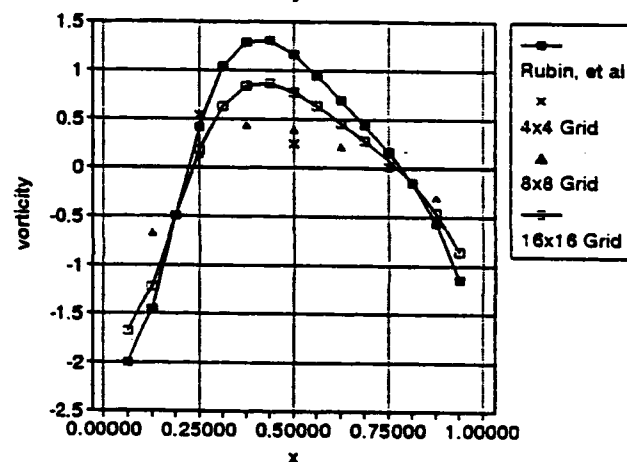
Vorticity versus x Position
at $y = 0.75$



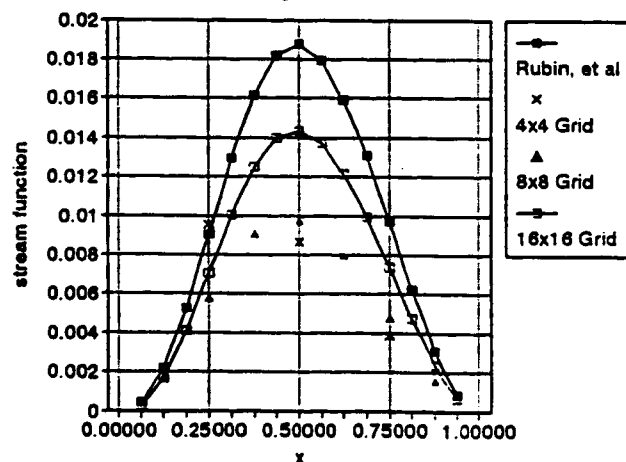
Stream Function versus x Position
at $y = 0.50$



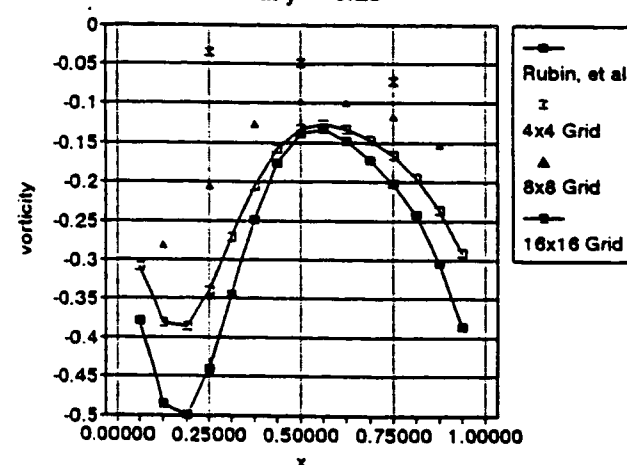
Vorticity versus x Position
at $y = 0.5$



Stream Function versus x Position
at $y = 0.25$



Vorticity versus x Position
at $y = 0.25$



Section 4

SOLUTION BY USE OF THE MATRIX EXPONENTIAL

This section describes the approach suggested by Dr. Shoosmith [Shoosmith]. The method involves solving Equation 3, a coupled system of first-order differential equations, by use of the matrix exponential. A sketch of how Shoosmith's method might be used to solve the above vector equations follows:

1. Use the initial values of ψ and ζ to construct the matrix $A(\psi)$ and the vector $\gamma(\psi)$.
2. Determine e^{At} , the "matrix exponential", which allows one to compute ζ at the $(k+1)$ -st time interval, given ζ at the k -th time interval by the equation

$$\zeta_{k+1} = e^{A(\Delta t)} \zeta_k + A^{-1} \left(e^{A(\Delta t)} - I \right) \gamma_k \quad (5)$$

3. Use equation (4) to solve for ψ_{k+1} .
4. Recompute the matrix $A(\psi)$ and vector $\gamma(\psi)$ using the updated ψ .
5. Iterate steps 2. through 4. until t_{final} .

A Pascal program, DCMEx (Driven Cavity by Matrix Exponential), was written to implement this solution scheme [Stafford]. Some specifics on how the algorithm described above were implemented are now presented.

The eigenvalues of $A(\psi)$ are assumed to be real and distinct for all ψ . They are computed by converting the A matrix to upper Hessenberg form and then applying the QR algorithm. The matrix A is then factored by a similarity transformation. The specific technique used is to (1) explicitly compute the right and left eigenvectors, (2) scale the left eigenvectors such that the product of each right and left eigenvector (for the same eigenvalue) is unity, and, (3) form two matrices S and T with the columns of S consisting of the right eigenvectors of $A(\psi)$ and the rows of T consisting of the scaled left

eigenvectors of $A(\psi)$. This results in T being an approximation to the inverse of S , and the matrix $A(\psi)$ is thus diagonalized--i.e., $A(\psi)$ can be written as the product

$$A = S \Lambda S^{-1}$$

with Λ being a diagonal matrix with the eigenvalues of A along its diagonal. The eigenvector computation is performed using the inverse power method (also called "inverse iteration") and, except for the first time step, the program uses the previous eigenvectors and eigenvalues as initial guesses for the new eigenvectors and eigenvalues. The number of iterations needed by the inverse iteration procedure is used to control the step size, the assumption being that if a pre-determined number of iterations is required then too large a step must have been attempted.

This, then, is a general description of the program written to implement the method proposed by Dr. Shoosmith. Unfortunately, the program was unsuccessful. When an equal number of row and column grid points were used the program was unable to factor $A(\psi)$ at the outset. It was suspected, and later confirmed, that the difficulty arose due to the existence of repeated eigenvalues. When an unequal number of horizontal and vertical grid points were used the program operated successfully for several iterations but eventually bogged down well before reaching a steady state. Checks of the eigenvalues seemed to indicate that although they began as real and distinct, the $A(\psi)$ values evolved in time to bring some pairs of eigenvalues close together. As these pairs came sufficiently close together they again caused problems in the inverse iteration process for finding the eigenvectors. In the following section the conventional method described in Section 3 is used to compute the spectrum of $A(\psi)$ as the solution progresses towards steady state. This allows a better understanding of why Shoosmith's method fails on this problem.

Section 5

SPECTRUM ANALYSIS OF THE COEFFICIENT MATRIX

Using the conventional methods to solve the driven cavity problem described in Section 3, and standard matrix eigenvalue computation techniques (reduction to upper Hessenberg form and QR iteration), the spectrum of the coefficient matrix in Equation 3 was obtained at several time instances during the solution process. Eigenvalue computations were carried out for grids having 9, 25, and 49 internal points (which correspond to interval widths of $1/4$, $1/6$, and $1/8$ unit, respectively), and the results are documented in Tables 1, 2, and 3, and depicted graphically in Figures 7, 8, and 9.

Several observations can be made. First, the eigenvalues of $A(\psi)$ at $t = 0$ are real and repeated for each grid coarseness. Second, the eigenvalues come off the real axis and become complex immediately after $t = 0$. (Although the first value of t displayed in the tables and figures is at $t = 1$, computations at the very first time interval in the simulation show the same characteristic.) Third, note that regardless of the grid coarseness the eigenvalue with largest real part (smallest real part in absolute value) is around -0.2 and remains reasonably close to this value from $t = 0$ through $t = 20$ where the system is essentially at steady state.

The first two observations above justify the claim in the previous section that the method of Dr. Shoosmith cannot be successful in solving the driven cavity problem because the eigenvalues are not real and distinct for all time. In fact, they are not real and distinct for any interval during the solution if the grid contains an equal number of horizontal and vertical intervals. Results for an unequal number of horizontal and vertical grid points ($N_x = 4$, $N_y = 3$) are displayed in Table 4. This table implies that although the spectrum begins with real and distinct roots, as time progresses some of the roots coalesce and become complex conjugate pairs. This corresponds precisely to the behavior exhibited by the program which implemented Dr. Shoosmith's method. The program ran nicely until the eigenvalues had nearly coalesced but then stalled as it was unable to compute eigenvectors when the spectrum contained nearly repeated eigenvalues. The third observation is remarkable because of its implications for computational

TABLE 1: SPECTRUM ANALYSIS OF 4X4 GRID

t = 0.0		t = 1.0		t = 20.0	
Real	Imag	Real	Imag	Real	Imag
-0.1875	0.0000	-0.1902	0.0000	-0.1987	0.0000
-0.4137	0.0000	-0.4176	-0.0521	-0.4374	-0.1420
-0.4137	0.0000	-0.4176	0.0521	-0.4374	0.1420
-0.6400	0.0000	-0.6400	0.0000	-0.6400	0.0000
-0.6400	0.0000	-0.6400	-0.0737	-0.6400	-0.1785
-0.6400	0.0000	-0.6400	0.0737	-0.6400	0.1785
-0.8663	0.0000	-0.8624	0.0521	-0.8426	0.1420
-0.8663	0.0000	-0.8624	-0.0521	-0.8426	-0.1420
-1.0925	0.0000	-1.0898	0.0000	-1.0813	0.0000

TABLE 2: SPECTRUM ANALYSIS OF 6X6 GRID

t = 0.0		t = 1.0		t = 20.0	
Real	Imag	Real	Imag	Real	Imag
-0.1929	0.0000	-0.2291	0.0000	-0.2360	0.0000
-0.4565	0.0000	-0.5049	0.1152	-0.5371	0.2055
-0.4565	0.0000	-0.5049	-0.1152	-0.5371	-0.2055
-0.7200	0.0000	-0.8163	0.2185	-0.8103	0.0000
-0.8165	0.0000	-0.8163	-0.2185	-0.8743	-0.3145
-0.8165	0.0000	-0.8548	0.0000	-0.8743	0.3145
-1.0800	0.0000	-1.1560	-0.3382	-1.1468	0.0719
-1.0800	0.0000	-1.1560	0.3382	-1.1468	-0.0719
-1.1765	0.0000	-1.1874	0.0186	-1.2020	0.4338
-1.1765	0.0000	-1.1874	-0.0186	-1.2020	-0.4338
-1.4400	0.0000	-1.4090	0.0000	-1.3289	0.0000
-1.4400	0.0000	-1.4400	0.0000	-1.4400	-0.6518
-1.4400	0.0000	-1.4400	-0.4491	-1.4400	0.0000
-1.4400	0.0000	-1.4400	0.4491	-1.4400	0.6518
-1.4400	0.0000	-1.4710	0.0000	-1.5511	0.0000
-1.7035	0.0000	-1.6926	0.0186	-1.6780	-0.4338
-1.7035	0.0000	-1.6926	-0.0186	-1.6780	0.4338
-1.8000	0.0000	-1.7240	-0.3382	-1.7332	0.0719
-1.8000	0.0000	-1.7240	0.3382	-1.7332	-0.0719
-2.0635	0.0000	-2.0252	0.0000	-2.0057	0.3145
-2.0635	0.0000	-2.0637	-0.2185	-2.0057	-0.3145
-2.1600	0.0000	-2.0637	0.2185	-2.0697	0.0000
-2.4235	0.0000	-2.3751	-0.1152	-2.3429	-0.2055
-2.4235	0.0000	-2.3751	0.1152	-2.3429	0.2055
-2.6871	0.0000	-2.6509	0.0000	-2.6440	0.0000

TABLE 3: SPECTRUM ANALYSIS OF 8X8 GRID

t = 0.0		t = 1.0		t = 20.0	
Real	Imag	Real	Imag	Real	Imag
-0.1949	0.0000	-0.2594	0.0000	-0.2644	0.0000
-0.4723	0.0000	-0.5520	-0.1064	-0.6353	-0.2320
-0.4723	0.0000	-0.5520	0.1064	-0.6353	0.2320
-0.7498	0.0000	-0.8764	0.2768	-0.9208	0.3829
-0.8876	0.0000	-0.8764	-0.2768	-0.9208	-0.3829
-0.8876	0.0000	-0.9826	0.0000	-0.9646	0.0000
-1.1651	0.0000	-1.2837	0.0000	-1.3349	0.0000
-1.1651	0.0000	-1.3298	-0.4653	-1.3373	0.6460
-1.3774	0.0000	-1.3298	0.4653	-1.3373	-0.6460
-1.3774	0.0000	-1.4494	0.0000	-1.4724	0.0000
-1.5803	0.0000	-1.7619	-0.0421	-1.7498	-0.1456
-1.6549	0.0000	-1.7619	0.0421	-1.7498	0.1456
-1.6549	0.0000	-1.8274	0.5932	-1.8366	0.8500
-1.8673	0.0000	-1.8274	-0.5932	-1.8366	-0.8500
-1.8673	0.0000	-1.9036	0.0000	-1.9276	0.0000
-2.0702	0.0000	-2.2044	0.1222	-2.2034	0.2307
-2.0702	0.0000	-2.2044	-0.1222	-2.2034	-0.2307
-2.1447	0.0000	-2.2865	0.0000	-2.2738	0.0000
-2.1447	0.0000	-2.2976	0.0000	-2.3323	0.0786
-2.2825	-0.0000	-2.3090	0.6996	-2.3323	-0.0786
-2.2825	0.0000	-2.3090	-0.6996	-2.3521	-0.9797
-2.5600	0.0000	-2.4882	0.0000	-2.3521	0.9797
-2.5600	0.0000	-2.5600	0.0000	-2.5600	-1.4696
-2.5600	0.0000	-2.5600	-0.9745	-2.5600	1.4696
-2.5600	0.0000	-2.5600	0.9745	-2.5600	0.0000
-2.5600	0.0000	-2.5600	0.2821	-2.5600	0.3541
-2.5600	0.0000	-2.5600	-0.2821	-2.5600	-0.3541
-2.5600	0.0000	-2.6318	0.0000	-2.7679	-0.9797
-2.8375	-0.0000	-2.8110	-0.6996	-2.7679	0.9797
-2.8375	0.0000	-2.8110	0.6996	-2.7877	0.0786
-2.9753	0.0000	-2.8224	0.0000	-2.7877	-0.0786
-2.9753	0.0000	-2.8335	0.0000	-2.8462	0.0000
-3.0498	0.0000	-2.9156	-0.1222	-2.9166	0.2307
-3.0498	0.0000	-2.9156	0.1222	-2.9166	-0.2307
-3.2527	0.0000	-3.2164	0.0000	-3.1924	0.0000
-3.2527	0.0000	-3.2926	-0.5932	-3.2834	0.8500
-3.4651	0.0000	-3.2926	0.5932	-3.2834	-0.8500
-3.4651	0.0000	-3.3581	0.0421	-3.3702	0.1456
-3.5397	0.0000	-3.3581	-0.0421	-3.3702	-0.1456
-3.7426	0.0000	-3.6706	0.0000	-3.6476	0.0000
-3.7426	0.0000	-3.7902	0.4653	-3.7827	0.6460
-3.9549	0.0000	-3.7902	-0.4653	-3.7827	-0.6460
-3.9549	0.0000	-3.8363	0.0000	-3.7851	0.0000
-4.2324	0.0000	-4.1374	0.0000	-4.1554	0.0000
-4.2324	0.0000	-4.2436	-0.2768	-4.1992	-0.3829
-4.3702	0.0000	-4.2436	0.2768	-4.1992	0.3829
-4.6477	0.0000	-4.5680	-0.1064	-4.4847	-0.2320
-4.6477	0.0000	-4.5680	0.1064	-4.4847	0.2320
-4.9251	0.0000	-4.8606	0.0000	-4.8556	0.0000

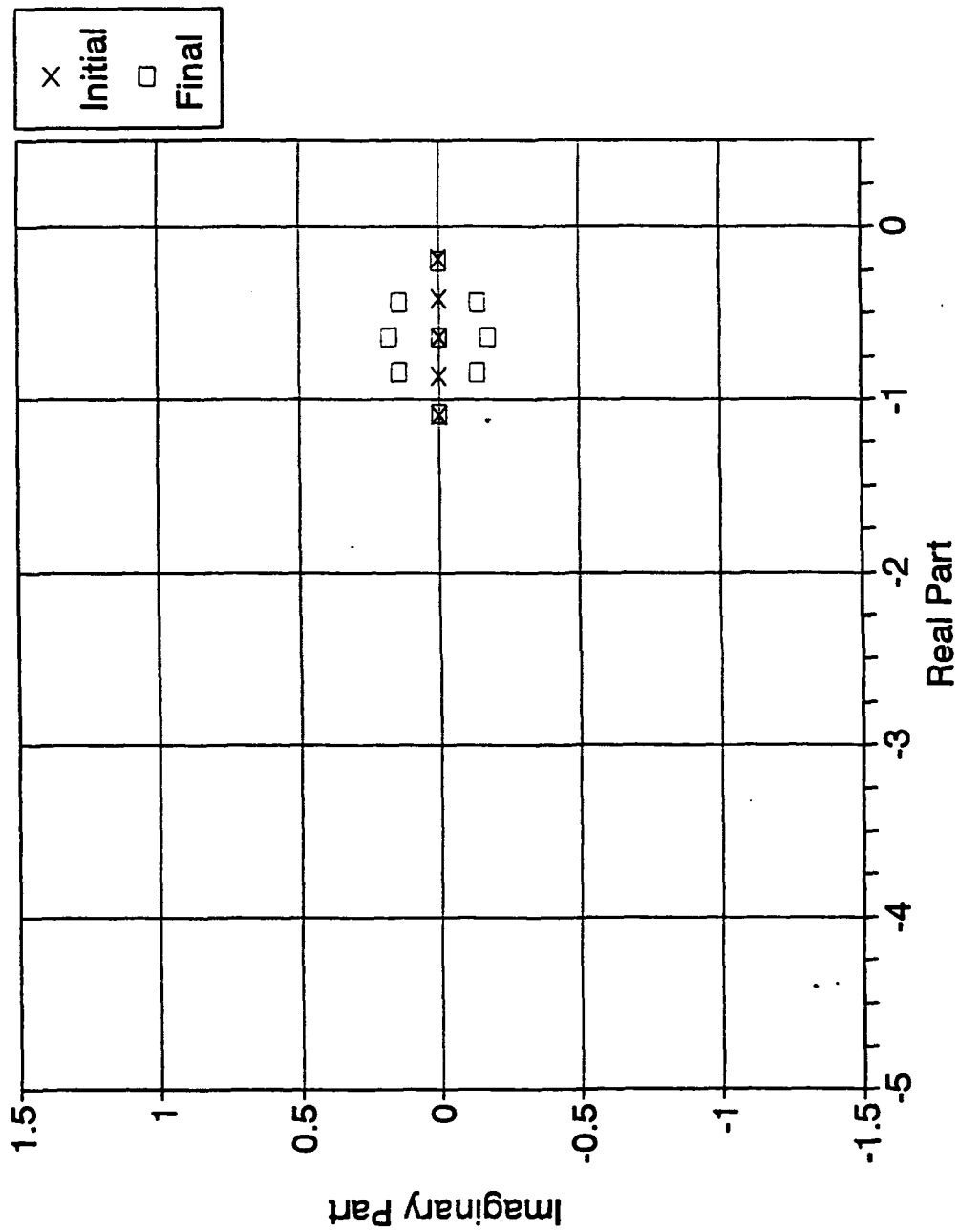


Figure 7: Eigenvalues for 4x4 Grid

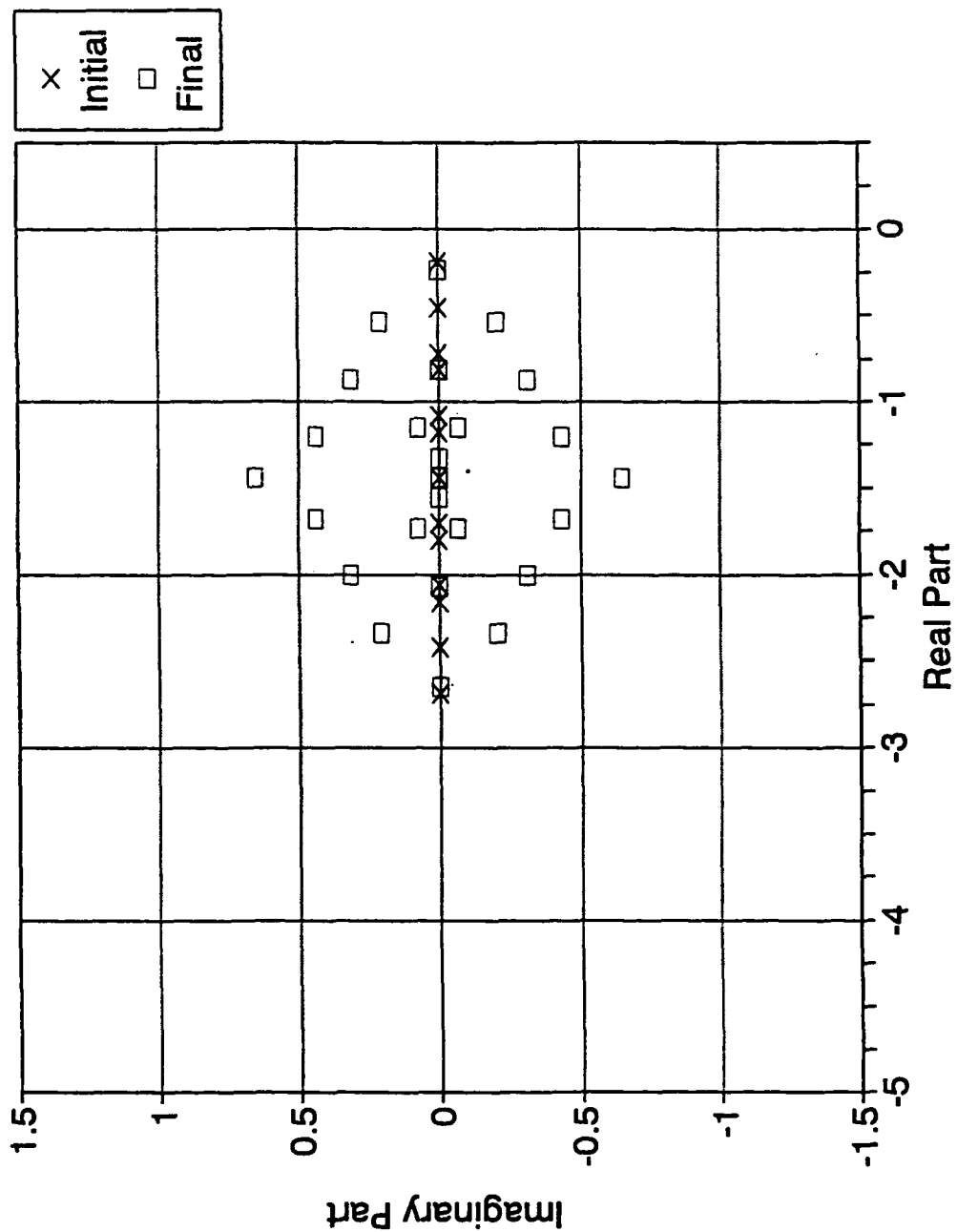


Figure 8: Eigenvalues for 6x6 Grid

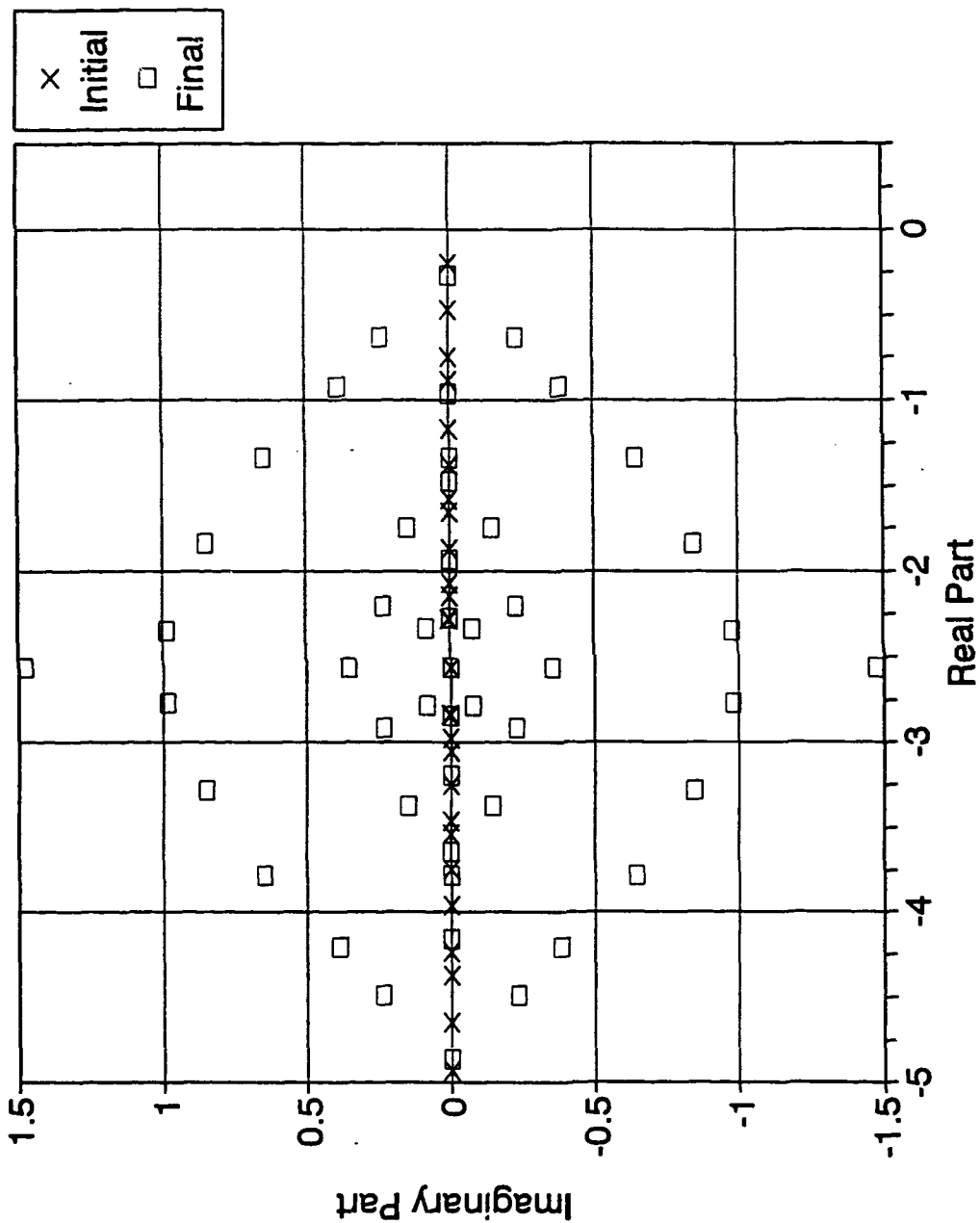


Figure 9: Eigenvalues for 8x8 Grid

TABLE 4: SPECTRUM ANALYSIS OF 4X3 GRID

t = 0.0		t = 0.05		t = 0.1		t = 0.2		t = 20.0	
Real	Imag	Real	Imag	Real	Imag	Real	Imag	Real	Imag
-0.18922	0	-0.18927	0	-0.18939	0	-0.18985	0.00000	-0.19967	0.00000
-0.41549	0	-0.41707	0	-0.42455	0	-0.42848	-0.01912	-0.45051	-0.13118
-0.43922	0	-0.43779	0	-0.43075	0	-0.42848	0.01912	-0.45051	0.13118
-0.64177	0	-0.64324	0	-0.64931	0	-0.65784	-0.01763	-0.73018	-0.20455
-0.66549	0	-0.66451	0	-0.66005	0	-0.65784	0.01763	-0.73018	0.20455
-0.74823	0	-0.74792	0	-0.74696	0	-0.74317	0.00000	-0.72290	0.00000
-0.89177	0	-0.89208	0	-0.89304	0	-0.89683	0.00000	-0.91710	0.00000
-0.97451	0	-0.97549	0	-0.97995	0	-0.98216	0.01763	-0.90982	0.20455
-0.99823	0	-0.99676	0	-0.99069	0	-0.98216	-0.01763	-0.90982	-0.20455
-1.20078	0	-1.20221	0	-1.20925	0	-1.2152	0.01912	-1.18949	0.13118
-1.22451	0	-1.22293	0	-1.21545	0	-1.21152	-0.01912	-1.18949	-0.13118
-1.45078	0	-1.45073	0	-1.45061	0	-1.45015	0.00000	-1.44033	0.00000

fluid dynamicists.

One can consider the system of first-order ordinary differential equations as a time varying linear system with a time-varying input vector. This is reasonable since ψ varies with time, and since A and γ vary with ψ , they are uniquely determined at every instant of time. A crude but perhaps useful approach to understanding the implication of the eigenvalue with smallest real part in absolute value is to partition the time interval from $t=0$ to the time when steady state is agreed to have occurred, $[0, t_{ss}]$, into intervals over which A is assumed to be constant. On each of these intervals the solution for ζ will contain a mode of the form $v_1 e^{\sigma t}$ where σ has a value close to -0.2 . If on any time interval the forcing function γ excites this mode, it is reasonable to expect that steady state will not occur until the time function $e^{\sigma t}$ has fallen to some reasonably small value. All other modes contain exponentials with more negative coefficients than -0.2 and hence their effects would die out sooner than the dynamics of this mode. Thus, the effect of this particular mode will tend to govern the time to steady state. Using a nominal value of 0.01 for $e^{\sigma t}$ we can make a crude estimate of the time for steady state to occur as follows:

$$e^{\sigma t_{ss}} \approx 0.01 \quad \Rightarrow \quad t_{ss} \approx - \frac{2 \ln(10)}{\sigma} \approx 23 \text{ sec}$$

where a value of $\sigma = -0.2$ has been used. Simulations in this report were all run to final times of 20 seconds, a value chosen somewhat arbitrarily but based loosely on the norm of the right hand side of Equation 3 becoming sufficiently small (approximately 10^{-5}). The value of 23 seconds predicted above is, then, a reasonable estimate of t_{ss} for this Reynolds number. Simulations were conducted with different Reynolds numbers and estimates of times to steady state were obtained by the same method as above. Those

estimates are contained in Table 5. Note that increasing the Reynolds number

Table 5: Estimates of Times to Steady State for Various Reynolds Numbers		
Reynolds Number	σ	Estimated t_{ss}
1	-19.49	0.24
10	- 1.949	2.4
100	- 0.1949	24.0
1000	- 0.01949	240.0

by a factor of 10 implies an increase by a factor of 10 in the time to steady state. Observations made during runs confirmed that the estimates in the table were reasonable, though no detailed numerical experiments were performed.

It is not difficult to show that the eigenvalues at the initial time vary in an uncomplicated fashion with Reynolds number. Let $A(\psi;R)$ represent the coefficient matrix $A(\psi)$ with Reynolds number R . By examining the ζ_ℓ equations we see that we can write

$$A(0;R) = \frac{1}{R\Delta x^2} K$$

where K is a 5-diagonal matrix with $K_{11} = -4$ and all other nonzero elements unity. The spectrum of K is easy to determine numerically. For the 3x3 grid we have the following eigenvalues of K :

$$\begin{aligned}\lambda_1 &\approx -1.172 \\ \lambda_2 &= \lambda_3 \approx -2.586 \\ \lambda_4 &= \lambda_5 = \lambda_6 \approx -4.000 \\ \lambda_7 &= \lambda_8 \approx -5.414 \\ \lambda_9 &\approx -6.828\end{aligned}$$

The eigenvalues at $t = 0$ for any Reynolds number can be determined by multiplying these values by $\frac{1}{R\Delta x^2}$. Thus, the smallest eigenvalue in absolute value for $R = 1, 10, 100$, and 1000 for the 3x3 grid becomes $\sigma = -18.75, -1.875, -0.1875$ and -0.01875 . Comparing these values with those in Table 5 we see that the change from initial to steady state in this critical value is always in the same proportion.

Section 6

CONCLUSION

This report has demonstrated conclusively that Dr. Shoosmith's method for parallelizing the numerical solution of systems of ordinary differential equations has serious limitations. This is unfortunate, since there is still no completely satisfactory method for taking advantage of parallel computers in solving systems of ODEs. As is usual with research, however, more questions have been raised than were answered during this investigation. Some of these questions and suggestions for further investigation are now offered.

Suggestions for Further Research

At the heart of the Shoosmith method is the use of inverse iteration to solve for eigenvectors of the coefficient matrix, $A(\psi)$, in parallel. It is perhaps possible to develop an efficient algorithm which would (1) detect the situation where eigenvalues are coalescing, (2) propagate the solution by an alternative method until the eigenvalues become complex, (3) compute eigenvectors or perhaps pairs of eigenvectors associated with these complex roots in parallel, and (4) continue propagating the solution in parallel. This appears to be a significant challenge, but tackling small systems (the 3x3 grid used in this report, for example) might provide insight into how one could proceed. If this is not possible, the method of Dr. Shoosmith will most likely never be competitive with more conventional serial methods because the classes of problems it would solve would be too restricted.

Other techniques for parallelizing the solution of systems of ODEs are being actively pursued, most notably the Krylov subspace methods proposed in [Gallopoulos]. This method was actually applied to the driven cavity problem in [Saad], but in the primitive variable formulation of the Navier Stokes equations. It would be interesting to apply the Krylov subspace method to the stream function-vorticity formulation of the Navier-Stokes equations. A comparison between the best conventional methods and a Krylov subspace method using the same grid coarseness might prove interesting.

The observations given in Section 5 relating to estimating the time to steady state need to be studied on more complicated geometries than just that of the driven cavity. The goal of such research would be to determine if the time to steady state is relatively insensitive to the shape of the boundary. Since computation of the eigenvalues of the $A(\psi)$ matrix on a coarse grid is computationally inexpensive, one could decide if solving for the steady state flow field by a time marching algorithm would be feasible for a given grid coarseness. Perhaps other methods for predicting the time to steady state for various Reynolds numbers already exist, but if not the results of this research should be communicated to the computational fluid dynamics community.

There are other trends to be observed from the spectrum analysis presented in Section 5. For example, the largest value of the imaginary parts of eigenvalues grew from runs made with 4x4 grids to 6x6 grids to 8x8 grids: the values were approximately 0.18, 0.65, and 1.5, respectively. These maximum imaginary parts correspond to the highest frequency component to be found in the solution for that particular grid coarseness. This information is perhaps useful, but three points are not sufficient to define exactly how the highest frequencies grow with increasingly finer grids. Another trend could be explored. It was noted that the time step required for stability in the conventional method described in Section 3 had to be considerably smaller as the Reynolds number increased on grids with the same coarseness. Typically, in computational fluid dynamics, capturing the flow details at high Reynolds numbers takes a finer grid and thus more computational time [Rubin]. Consequently, it is natural to ask if there exists any information in the spectrum of $A(\psi)$ which would suggest how to overcome this. Also, can we predict a reasonable time step size by performing a preliminary analysis of the spectrum?

Finally, the work contained in this report could be useful for several purposes not originally envisioned. While the driven cavity problem is discussed considerably in the literature, this report provides a more detailed development of the equations than one would generally find in refereed articles, thereby making this interesting problem more accessible to faculty and students. At USAFA the Department of Mathematica Sciences offers a course in numerical analysis. Additionally, the Department of Aeronautics uses

computational fluid dynamics in several of their aerodynamics courses. Much of the tedious work needed to develop and verify the equations for the driven cavity problem has been done and documented herein. Consequently, instructors may find the driven cavity problem to be sufficiently challenging and interesting to be used in conjunction with their classes. Different Poisson solvers could be compared, for example, with the Gauss-Seidel method used in this report. Also, performance of implicit ODE solvers might be compared with that of the Runge-Kutta method. A better physical understanding of the Navier-Stokes equations might also be gained using the methods in this report to solve this problem numerically. From the numerical results, students can then determine, for example, steady state velocity and pressure distributions within the cavity.

REFERENCES

Ames, William F. *Numerical Methods for Partial Differential Equations*. 2nd ed. New York, N.Y. Academic Press, 1977.

Gallopoulos, E. and Y. Saad. *On the Parallel Solution of Parabolic Equations*. NASA Ames Research Center, CA: Research Institute for Advanced Computer Science. RIACS Technical Report 89.19, 1989.

Rubin, Stanley G., et al. *Numerical Studies of Incompressible Viscous Flow in a Driven Cavity*. Washington, D.C: National Aeronautics and Space Administration SP-378, 1975.

Saad, Y. and B. D. Semeraro. "Application of Kryolv Exponential Propagation to Fluid Dynamics Equations." Conference Proceedings (AIAA-91-1567-CP), American Institute of Aeronautics and Astronautics, Inc., 1991.

Shoosmith, John N. "Explicit Numerical Solution of Initial Value Problems on Parallel Computers." Project write-up for the Analysis and Computation Division, NASA Langley Research Center, 1991.

Stafford, Max A. "Programmer's Guide to Accompany DCMEx." US Air Force Academy, CO: Unpublished report, 1991.

APPENDIX A

Equations Arising from the Method of Lines Applied to the Driven Cavity Problem

In Section 2 the driven cavity problem was defined and a sample derivation of equations arising from the method of lines was given. In this appendix the complete set of equations used in all simulations is presented. The symbol R is used throughout to denote the Reynolds number. The symbol h is used to denote the ratio of the uniform interval widths in the y direction, Δy , to the uniform widths in the x direction, Δx : $h = \Delta y / \Delta x$.

Node at Lower Left Corner:

$$\begin{aligned} \dot{\zeta}_\ell &= \frac{-2}{h^2 \Delta x^2 R} \left(1 + h^2 \right) \zeta_\ell + \frac{1}{4h^2 \Delta x^2 R} \left(4h^2 - hR\psi_{\ell+N_x} \right) \zeta_{\ell+1} \\ &+ \frac{1}{4h^2 \Delta x^2 R} \left(4 + hR\psi_{\ell+1} \right) \zeta_{\ell+N_x} \\ &+ \frac{\psi_\ell}{2h^4 \Delta x^4 R} \left[-4(1 + h^4) + hR\psi_{\ell+1} - h^3 R\psi_{\ell+N_x} \right] \\ \frac{1}{h^2 \Delta x^2} &\left(-2(1 + h^2)\psi_\ell + h^2\psi_{\ell+1} + \psi_{\ell+N_x} \right) = -\zeta_\ell \end{aligned}$$

Node on Bottom Interior:

$$\begin{aligned}
 \dot{\zeta}_\ell &= \frac{1}{4h^2 \Delta x^2 R} \left(4h^2 + hR\psi_{\ell+N_x} \right) \zeta_{\ell-1} \\
 &+ \frac{-2}{h^2 \Delta x^2 R} \left(1 + h^2 \right) \zeta_\ell + \frac{1}{4h^2 \Delta x^2 R} \left(4h^2 - hR\psi_{\ell+N_x} \right) \zeta_{\ell+1} \\
 &+ \frac{1}{4h^2 \Delta x^2 R} \left(4 + hR(\psi_{\ell+1} - \psi_{\ell-1}) \right) \zeta_{\ell+N_x} \\
 &+ \frac{\psi_\ell}{2h^4 \Delta x^4 R} \left[-4 + hR(\psi_{\ell+1} - \psi_{\ell-1}) \right] \\
 \\
 \frac{1}{h^2 \Delta x^2} \left(h^2 \psi_{\ell-1} - 2(1 + h^2) \psi_\ell + h^2 \psi_{\ell+1} + \psi_{\ell+N_x} \right) &= -\zeta_\ell
 \end{aligned}$$

Node at Lower Right Corner:

$$\begin{aligned}
 \dot{\zeta}_\ell &= \frac{1}{4h^2 \Delta x^2 R} \left(4h^2 + hR\psi_{\ell+N_x} \right) \zeta_{\ell-1} + \frac{-2}{h^2 \Delta x^2 R} \left(1 + h^2 \right) \zeta_\ell \\
 &+ \frac{1}{4h^2 \Delta x^2 R} \left(4 - hR\psi_{\ell-1} \right) \zeta_{\ell+N_x} \\
 &+ \frac{\psi_\ell}{2h^4 \Delta x^4 R} \left[-4(1 + h^4) - hR\psi_{\ell-1} + h^3 R\psi_{\ell+N_x} \right] \\
 \\
 \frac{1}{h^2 \Delta x^2} \left(h^2 \psi_{\ell-1} - 2(1 + h^2) \psi_\ell + \psi_{\ell+N_x} \right) &= -\zeta_\ell
 \end{aligned}$$

Node on Right Interior:

$$\begin{aligned}
 \dot{\zeta}_\ell &= \frac{1}{4h^2\Delta x^2R} \left(4 + hR\psi_{\ell-1} \right) \zeta_{\ell-N_x} \\
 &+ \frac{1}{4h^2\Delta x^2R} \left(4h^2 + hR(\psi_{\ell+N_x} - \psi_{\ell-N_x}) \right) \zeta_{\ell-1} + \frac{-2}{h^2\Delta x^2R} \left(1 + h^2 \right) \zeta_\ell \\
 &+ \frac{1}{4h^2\Delta x^2R} \left(4 - hR\psi_{\ell-1} \right) \zeta_{\ell+N_x} \\
 &+ \frac{\psi_\ell}{2h^4\Delta x^4R} \left[-4h^4 + h^3R(\psi_{\ell+N_x} - \psi_{\ell-N_x}) \right] \\
 &\frac{1}{h^2\Delta x^2} \left(\psi_{\ell-N_x} + h^2\psi_{\ell-1} - 2(1 + h^2)\psi_\ell + \psi_{\ell+N_x} \right) = -\zeta_\ell
 \end{aligned}$$

Node at Upper Right Corner:

$$\begin{aligned}
 \dot{\zeta}_\ell &= \frac{1}{4h^2\Delta x^2R} \left(4 + hR\psi_{\ell-1} \right) \zeta_{\ell-N_x} \\
 &+ \frac{1}{4h^2\Delta x^2R} \left(4h^2 - hR\psi_{\ell-N_x} \right) \zeta_{\ell-1} + \frac{-2}{h^2\Delta x^2R} \left(1 + h^2 \right) \zeta_\ell \\
 &+ \frac{\psi_\ell}{2h^4\Delta x^4R} \left[-4(1 + h^4) - h^3R\psi_{\ell-N_x} + hR\psi_{\ell-1} \right] \\
 &+ \frac{1}{2h^3\Delta x^3R} \left(4 - hR\psi_{\ell-1} \right) \\
 &\frac{1}{h^2\Delta x^2} \left(\psi_{\ell-N_x} + h^2\psi_{\ell-1} - 2(1 + h^2)\psi_\ell \right) = -\zeta_\ell
 \end{aligned}$$

Node on Top Interior:

$$\begin{aligned}
 \dot{\zeta}_\ell &= \frac{1}{4h^2\Delta x^2R} \left(4 - hR(\psi_{\ell+1} - \psi_{\ell-1}) \right) \zeta_{\ell-N_x} + \frac{1}{4h^2\Delta x^2R} \left(4h^2 - hR\psi_{\ell-N_x} \right) \zeta_{\ell-1} \\
 &+ \frac{-2}{h^2\Delta x^2R} \left(1 + h^2 \right) \zeta_\ell + \frac{1}{4h^2\Delta x^2R} \left(4h^2 + hR\psi_{\ell-N_x} \right) \zeta_{\ell+1} \\
 &+ \frac{\psi_\ell}{2h^4\Delta x^4R} \left[-4 - hR(\psi_{\ell+1} - \psi_{\ell-1}) \right] \\
 &+ \frac{\psi_\ell}{2h^3\Delta x^3R} \left[4 + hR(\psi_{\ell+1} - \psi_{\ell-1}) \right] \\
 &\frac{1}{h^2\Delta x^2} \left(\psi_{\ell-N_x} + h^2\psi_{\ell-1} - 2(1 + h^2)\psi_\ell + h^2\psi_{\ell+1} \right) = -\zeta_\ell
 \end{aligned}$$

Node at Upper Left Corner:

$$\begin{aligned}
 \dot{\zeta}_\ell &= \frac{1}{4h^2\Delta x^2R} \left(4 - hR\psi_{\ell+1} \right) \zeta_{\ell-N_x} + \frac{-2}{h^2\Delta x^2R} \left(1 + h^2 \right) \zeta_\ell \\
 &+ \frac{1}{4h^2\Delta x^2R} \left(4h^2 + hR\psi_{\ell-N_x} \right) \zeta_{\ell+1} \\
 &+ \frac{\psi_\ell}{2h^4\Delta x^4R} \left[-4(1 + h^4) - h^3R\psi_{\ell-N_x} - hR\psi_{\ell+1} \right] \\
 &+ \frac{1}{2h^3\Delta x^3R} \left(4 + hR\psi_{\ell+1} \right) \\
 &\frac{1}{h^2\Delta x^2} \left(\psi_{\ell-N_x} - 2(1 + h^2)\psi_\ell + h^2\psi_{\ell+1} \right) = -\zeta_\ell
 \end{aligned}$$

Node on Left Interior:

$$\begin{aligned}
 \dot{\zeta}_\ell &= \frac{1}{4h^2 \Delta x^2 R} \left(4 - hR\psi_{\ell+1} \right) \zeta_{\ell-N_x} + \frac{-2}{h^2 \Delta x^2 R} \left(1 + h^2 \right) \zeta_\ell \\
 &+ \frac{1}{4h^2 \Delta x^2 R} \left(4h^2 - hR(\psi_{\ell+N_x} - \psi_{\ell-N_x}) \right) \zeta_{\ell+1} \\
 &+ \frac{1}{4h^2 \Delta x^2 R} \left(4 + hR\psi_{\ell+1} \right) \zeta_{\ell+N_x} \\
 &+ \frac{\psi_\ell}{2h^4 \Delta x^4 R} \left[-4h^4 - h^3 R(\psi_{\ell+N_x} - \psi_{\ell-N_x}) \right] \\
 &\frac{1}{h^2 \Delta x^2} \left(\psi_{\ell-N_x} - 2(1 + h^2)\psi_\ell + h^2\psi_{\ell+1} + \psi_{\ell+N_x} \right) = -\zeta_\ell
 \end{aligned}$$

Node on Interior:

$$\begin{aligned}
 \dot{\zeta}_\ell &= \frac{1}{4h^2 \Delta x^2 R} \left(4 - hR(\psi_{\ell+1} - \psi_{\ell-1}) \right) \zeta_{\ell-N_x} \\
 &+ \frac{1}{4h^2 \Delta x^2 R} \left(4h^2 + hR(\psi_{\ell+N_x} - \psi_{\ell-N_x}) \right) \zeta_{\ell-1} \\
 &+ \frac{-2}{h^2 \Delta x^2 R} \left(1 + h^2 \right) \zeta_\ell \\
 &+ \frac{1}{4h^2 \Delta x^2 R} \left(4h^2 - hR(\psi_{\ell+N_x} - \psi_{\ell-N_x}) \right) \zeta_{\ell+1} \\
 &+ \frac{1}{4h^2 \Delta x^2 R} \left(4 + hR(\psi_{\ell+1} - \psi_{\ell-1}) \right) \zeta_{\ell+N_x} \\
 &\frac{1}{h^2 \Delta x^2} \left(\psi_{\ell-N_x} + h^2\psi_{\ell-1} - 2(1 + h^2)\psi_\ell + h^2\psi_{\ell+1} + \psi_{\ell+N_x} \right) = -\zeta_\ell
 \end{aligned}$$

APPENDIX B

APPROXIMATE SOLUTIONS TO DRIVEN CAVITY PROBLEM

x	Rubin	zeta at y = 0.25		
		4x4 Grid	8x8 Grid	16x16 Grid
0.00000				
0.06250	-0.3786			-0.30814
0.12500	-0.4857		-0.28139	-0.38188
0.18750	-0.4998			-0.38597
0.25000	-0.4411	-0.03565	-0.20528	-0.34008
0.31250	-0.3449			-0.27175
0.37500	-0.2481		-0.12678	-0.20586
0.43750	-0.1763			-0.15785
0.50000	-0.1393	-0.04945	-0.09661	-0.13248
0.56250	-0.1338			-0.12657
0.62500	-0.1486		-0.09941	-0.13332
0.68750	-0.1729			-0.14698
0.75000	-0.2026	-0.07218	-0.11650	-0.16628
0.81250	-0.2429			-0.19480
0.87500	-0.3038		-0.15311	-0.23705
0.93750	-0.3869			-0.29086
1.00000				

x	Rubin	zeta at y = 0.5		
		4x4 Grid	8x8 Grid	16x16 Grid
0.00000				
0.06250	-2.003			-1.67875
0.12500	-1.453		-0.68215	-1.22305
0.18750	-0.4999			-0.49712
0.25000	0.4174	0.53867	0.13994	0.17619
0.31250	1.034			0.62608
0.37500	1.291		0.42900	0.83624
0.43750	1.304			0.86333
0.50000	1.163	0.23901	0.38380	0.77608
0.56250	0.9431			0.62927
0.62500	0.6923		0.21847	0.45747
0.68750	0.4336			0.27544
0.75000	0.1633	0.01852	0.00636	0.07885
0.81250	-0.1518			-0.15454
0.87500	-0.5698		-0.29700	-0.45846
0.93750	-1.146			-0.86118
1.00000				

x	Rubin	zeta at y = 0.75		
		4x4 Grid	8x8 Grid	16x16 Grid
0.00000				
0.06250	-3.868			-2.99578
0.12500	1.649		2.60673	1.75368
0.18750	3.887			3.58481
0.25000	4.109	2.80310	2.78029	3.80277
0.31250	3.748			3.44705
0.37500	3.271		2.07229	2.94137
0.43750	2.785			2.42719
0.50000	2.313	0.37904	1.31124	1.94826
0.56250	1.861			1.51369
0.62500	1.424		0.74053	1.11720
0.68750	0.9865			0.74171
0.75000	0.5156	0.34140	0.26235	0.35765
0.81250	-0.05295			-0.08234
0.87500	-0.8273		-0.31194	-0.64903
0.93750	-1.934			-1.42992
1.00000				

x	Rubin	psi at y = 0.25		
		4x4 Grid	8x8 Grid	16x16 Grid
0.00000				
0.06250	4.72200E-04			3.12544E-04
0.12500	2.21900E-03		1.68049E-03	1.70100E-03
0.18750	5.24800E-03			4.10614E-03
0.25000	9.07400E-03	9.55538E-03	5.78823E-03	7.09378E-03
0.31250	1.29600E-02			1.00698E-02
0.37500	1.61700E-02		9.05850E-03	1.24858E-02
0.43750	1.81900E-02			1.39684E-02
0.50000	1.87900E-02	8.68265E-03	9.73202E-03	1.43601E-02
0.56250	1.79700E-02			1.36939E-02
0.62500	1.59500E-02		7.93981E-03	1.21371E-02
0.68750	1.30700E-02			9.93331E-03
0.75000	9.69900E-03	3.87427E-03	4.75398E-03	7.36243E-03
0.81250	6.23300E-03			4.72794E-03
0.87500	3.11700E-03		1.55483E-03	2.36728E-03
0.93750	8.59600E-04			6.61075E-04
1.00000				

x	Rubin	psi at y = 0.5	
		4x4 Grid	8x8 Grid
0.00000			
0.06250	3.88300E-03		
0.12500	1.48400E-02		1.24731E-02
0.18750	2.99400E-02		
0.25000	4.52000E-02	3.17669E-02	2.85576E-02
0.31250	5.74600E-02		
0.37500	6.51300E-02		3.64173E-02
0.43750	6.79100E-02		
0.50000	6.62600E-02	2.43918E-02	3.49585E-02
0.56250	6.09900E-02		
0.62500	5.30000E-02		2.72142E-02
0.68750	4.31400E-02		
0.75000	3.22400E-02	1.13257E-02	1.65020E-02
0.81250	2.11600E-02		
0.87500	1.09700E-02		5.95756E-03
0.93750	3.20300E-03		
1.00000			

psi at y = 0.75			
0.00000			
0.06250	1.51400E-02		
0.12500	4.52100E-02		4.78548E-02
0.18750	7.21500E-02		
0.25000	9.01300E-02	5.94535E-02	6.70206E-02
0.31250	9.98400E-02		
0.37500	1.03000E-01		6.74914E-02
0.43750	1.01300E-01		
0.50000	9.56700E-02	3.08536E-02	5.75064E-02
0.56250	8.70800E-02		
0.62500	7.61400E-02		4.30256E-02
0.68750	6.32900E-02		
0.75000	4.89100E-02	1.58792E-02	2.67681E-02
0.81250	3.35300E-02		
0.87500	1.82500E-02		1.07792E-02
0.93750	5.55400E-03		
1.00000			